Science

MEDUSA: Observation of atmospheric dust and water vapor close to the surface of Mars

F. Esposito[1], L. Colangeli[2], V. Della Corte[3], C. Molfese[1], P. Palumbo[3], S. Ventura[4], J. Merrison[5], P. Nørnberg[5], J. F. Rodriguez-Gomez[6], J. J. Lopez-Moreno[6], B. del Moral[6], J. M. Jerónimo[6], R. Morales[6], E. Battistelli[7], S. Gueli[7], R. Paolinetti[7] and the International MEDUSA Team

[1]INAF-Osservatorio Astronomico di Capodimonte, Naples, 80131, Italy, *francesca.esposito@na.astro.it*; [2] *Solar System Missions Division – Research and Scientific Support Department – European Space Agency – ESTEC, Keplerlaan 1 – PO Box 299 – 2200 AG Noordwijk ZH – The Netherlands;*[3] *Dept. of Applied Science, University of Naples "Parthenope", Naples, 80143, Italy;* [4]*University of Naples "Federico II", Naples, 80125, Italy;* [5]*Mars Simulation Laboratory, Institute for Physics and Astronomy, Aarhus, 8000C, Denmark;* [6]*Instituto de Astrofisica de Andalucia CSIC, Granada, 19008, Spain;* [7]*Selex Galileo, Campi Bisenzio (FI), 50013, Italy.*

Abstract

Background: The study of airborne dust and water vapor properties at the Martian surface level is an important task for the achievement of some of the primary scientific goals of Mars exploration: to study the water cycle and present / past habitability, climate history and hazardous conditions.

Method: The MEDUSA instrument has been designed for the direct *in situ* measurement of dust and water vapor properties, such as dust size distribution, number density, deposition rate and electrification, and water vapor abundance.

Conclusion: The MEDUSA instrument reached a Technical Readiness Level > 5 within the ESA ExoMars mission development and it is well suited to be accommodated on landers and rovers for Mars exploration.

Introduction

Dust and water vapor are fundamental components of the Martian atmosphere. In view of tracing the past Mars environmental conditions, that possibly favored the appearing of life forms, it is important to study the present climate and its evolution. Of major scientific interest are the abundance and physical, chemical and electrical properties of dust, the abundance of water vapor dispersed in the atmosphere and its exchange with the surface. Moreover, in view of the future exploration of the planet, it is of primary importance to analyze the hazards linked to environmental factors. The Martian Environmental Dust Systematic Analyzer (MEDUSA) experiment has been developed for the characterization of airborne dust and water vapor close to the surface of Mars and is suitable to be accommodated on Martian landers or rovers. MEDUSA implements a suite of optical and piezoelectric sensors aimed to measure, for the first time, in-situ and quantitatively, the atmospheric water

vapor abundance and the following dust properties: size distribution, number density vs. size, cumulative mass flux, deposition rate, electrification. All these properties can be monitored as a function of time, allowing the study of their evolution during local events and diurnal / seasonal cycles.

Scientific rationale

Studying dust close to the surface of Mars

Dust is permanently present in the atmosphere of Mars. Its amount varies with seasons and with the presence of local and global dust storms. Airborne dust contributes to determine the dynamic and thermodynamic evolution of the atmosphere (Zurek et al. 1992), including large scale circulation processes, on diurnal, seasonal and annual time-scales (Smith 2008). It plays a key role in determining the current climate of Mars and probably influenced the past climatic conditions and surface evolution. Dust grains absorb

and scatter thermal and solar radiation and act as condensation nuclei for H_2O and CO_2, so influencing the atmospheric thermal structure, balance and circulation (James et al 1992; Jakosky and Haberle 1992; Kahn et al 1992; Ryan and Henry 1979; Forget et al. 2006; Martin and Kieffer 1979; Martin 1981; Jakosky and Martin 1987). Main parameters influencing the atmospheric heating are size distribution, albedo, single scattering phase function and imaginary part of the refractive index. Moreover, wind and windblown dust represent nowadays the most active processes having long term effects on Martian geology and morphological evolution (Greeley et al. 1992). Aeolian erosion, dust redistribution on surface and weathering are mechanisms coupling surface and atmospheric evolution and are driven by wind intensity and grain properties. Wind mobilized particles on Mars range in size from less than 1 µm, for suspended dust, to perhaps as large as 1 cm in diameter. The mechanisms for dust entrainment in the atmosphere are not completely understood as the data available so far do not allow us to identify the efficiency of proposed processes. Wind tunnel experiments show that sand-size particles are easier to entrain than dust (Greeley and Iversen 1985). So, a first model for dust injection required sandblasting (Iversen and White 1982), where *saltating* sand-size particles are responsible for dust entrainment via impacts. Anyway, despite large evidences of sand-size grains on the Martian surface, recent observations show that sand movements are rare nowadays with respect to dust lifting (Zurek and Martin 1993; Cantor et al. 2002; Zimbelman 2000; Malin and Edgett 2001; Fenton 2006; Bourke et al. 2008; Chojnacki et al. 2010; Silvestro et al. 2010). MER Microscopic Imager observations have shown that surface dust occurs as fragile, low-density, sand-sized aggregates (Sullivan et al. 2008). Supposing these dust aggregates are widespread on Martian dusty regions, Sullivan et al. tried to resolve the paradox proposing that they could be the primary source of airborne dust as they are entrained and disrupted more easily than clay-sized (generally < 4 µm) air fall particles. In this case (sand-sized diameters and very low densities), the classic Iversen & White relationships (Iversen and White 1982) predict much lower thresholds for wind speed to mobilize dust. The creation dynamics of such dust aggregates are intimately related to grain electrification and show that grain size is a dynamic and highly variable parameter (Merrison et al. 2004; Merrison et al. 2007). The transport of dust can be quantitatively understood only through direct study from the Martian surface.

Information about the size distribution of atmospheric dust on Mars has been mainly retrieved from remote optical measurements (*e.g.*, Toon et al. 1977; Drossart et al. 1991; Pollack et al. 1995; Tomasko et al. 1999 – see Figure 1). It is still not known what the primary airborne dust (*e.g.*, the recently lifted dust) is made of, size-wise.

The number density of particles close to the Martian surface is n = 1 - 2 cm^{-3} in constant haze (Moroz et al. 1993). Metzger et al. (1999) quoted a dust mass density of 1.8×10^{-7} kg m^{-3} in standard conditions and 7×10^{-5} kg m^{-3} during a

dust devil. This density corresponds to n = 2 cm^{-3} and n = 1500 cm^{-3}, respectively, for particles with r = 1.6 µm and r = 2.6 g cm^{-3}.

Beside its scientific interest, the study of atmospheric Martian dust is relevant in the context of analyzing hazard connected to the contamination/failure of payloads in space missions (*e.g.*, solar panels, mechanisms, optical systems) and to the environmental risks for human exploration, due to dust deposition, impacts and electrification.

The measurement *in situ* of the amount, mass/size distribution, deposition rate, dynamical properties and electrification of solid particles in the Martian atmosphere, as a function of time, is a fundamental step. It may shade light on climatic processes, and in particular on the airborne dust evolution, and will help to prepare for future missions to Mars.
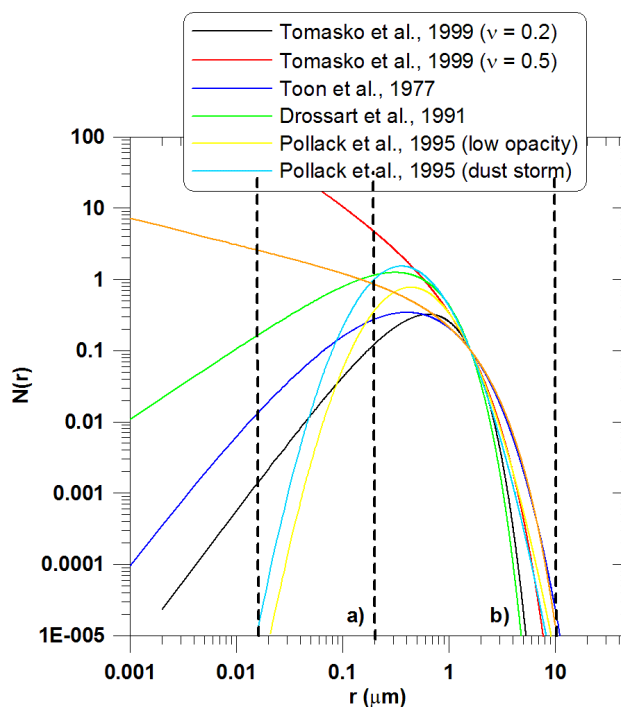

Figure 1. Comparison of dust size distributions in the Mars atmosphere as derived by various authors. Curves are scaled for N = 0.1 at grain radius r = 1.6 µm. Dashed lines indicate the MEDUSA size measurement ranges: the range a), from 0.05 to 0.2 µm, is covered by cumulative measurements, the range b), from 0.2 to 10 µm, is covered by single grain detections.

Studying water vapor close to the surface of Mars

Although water vapor is a minor constituent of the Martian atmosphere it plays a fundamental role. It is a primary indicator of seasonal climatic behavior, linked to the exchange with surface natural reservoirs (polar caps, regolith) and to atmospheric transport mechanisms.

The information on abundance and distribution of water vapor available so far is based on ground and remote

observations. Viking, Mars Global Surveyor (MGS), Mars Express and Mars Reconnaissance Orbiter (MRO) missions collected global information on atmospheric water-cycle (Jakosky and Farmer 1982; Smith 2002; Fedorova et al. 2006; Fedorova et al. 2009; Melchiorri et al. 2007; Smith et al. 2009), while the Mars Pathfinder (Titov et al. 1999), the Mars Exploration Rovers (Smith et al. 2004) and Phoenix (Whiteway et al. 2009) gave local measurements at the Martian surface. The distribution of water vapor varies with latitude and seasons. The annual average is 17 pr-μm in the latitude band 10° S - 40° N, and 12 pr-μm elsewhere, as computed from MGS Thermal Emission Spectrometer (TES) data, referencing the water vapor abundance to a 6.1 mbar pressure at surface (Smith 2002). Measurements from orbit show a maximum concentration at high latitudes during northern hemisphere summer. This is due to sublimation of water ice present in the polar region. After L_s = 120 the concentration is observed to decrease rapidly at high northern latitudes and to increase at low northern latitudes. This implies an equator-ward transport of water vapor. In the southern hemisphere, a high latitude summertime maximum is observed, about half of that observed in the north.

Polar regions are not the only source of water vapor. Another important natural reservoir is the regolith. Generally, a positive correlation has been observed between water vapor abundance and surface albedo, while a negative trend is observed with thermal inertia (Smith et al. 2009; Jakosky and Farmer 1982; Rosenqvist et al. 1992; Smith 2002). Moreover, recent results from the Mars Express Planetary Fourier Spectrometer (Fouchet et al. 2007; Tschimmel et al. 2008) show high concentration of water vapor over the regions of Arabia Terra and Tharsis, implying a possible local exchange of water between surface and atmosphere. Measurements performed *in situ* by instruments on-board rovers and/or landers give local detailed information about water vapor diurnal cycle. They show constant interaction between soil, water ice and vapor (*e.g.*, Smith et al. 2009). These elements suggest the importance of studying in situ water vapor content close to the surface and its atmosphere-surface exchanges. Further local monitoring and modeling (Saruya et al. 2010) are needed in order to shed light on the exchange mechanisms.

The MEDUSA instrument

The MEDUSA instrument is a suite of sensors for the characterization of atmospheric dust and water vapor at surface level. The goals of the MEDUSA experiment are to study *in situ,* directly and quantitatively the cumulative dust mass flux and dust deposition rate, the physical and electrification properties, the size distribution and number density of sampled particles and the water vapor abundance versus time, a goal that has never been achieved so far.

The information that can be obtained by *in situ* measurements over different time spans (days, seasons, years) represents a key input in different areas of interest.

In Mars science:

- To determine present climatic conditions at Mars surface

- To derive information about past history of Mars climate

- To search for water reservoirs

- To determine physical parameters impacting on life presence on Mars

- To provide ground-truth for validation of data coming from orbiter observations

In Mars operations:

- To evaluate hazardous conditions due to Martian environment

- To place constraints on operative conditions at Mars

- To support the definition of future Mars exploration missions

The MEDUSA experiment is based on the coupling of different techniques using optical detection and cumulative mass deposition. It consists in a dust collector (Main Body – envelope: 130 mm Ø ´ 187 mm h), and two separate stages for water vapor monitoring (MBwv - envelope: 30 mm ´ 50 mm Ø) and for dust deposition and electrification measurement (DDES - envelope: 120 mm Ø ´ 45 mm h), as shown in Figure 2. The Main Body, the MBwv and the DDES subsystems have to be individually accommodated on the rover/lander, with dedicated mechanical interfaces.
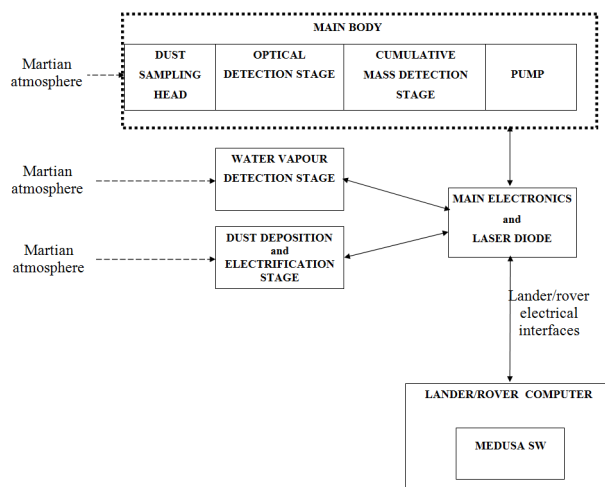

Figure 2. MEDUSA functional block diagram.

MEDUSA returns directly physical parameters of dust and water vapor in the Mars atmosphere as reported in Figure 3.

Starting from the quantities directly measured by MEDUSA, important information is derived about dust and water vapor, as illustrated below.

Atmospheric dust particle size distribution. MEDUSA is able to measure the size of atmospheric dust in a wide size range (from 0.01 to 10 μm); complementary techniques covering different size ranges are coupled. MEDUSA is able to detect optically single particles ≥ 0.2 μm in radius and to measure

3

Sensor	Primary Output	Derived Output
Dust Optical Detector	Scattered light in forward	Dust concentration
	Scattered light in backward	Grain size and shape
	Time of flight	Grain optical properties
Dust Collector based on microbalance	Dust mass in size range	Dust concentration
Water Vapour Detector based on microbalance	Collected water vapour	Humidity
Dust Deposition and Electrification Sensor based on 6 lasers + photodiodes + electrical field	Deposition of dust	Electrification of dust
	Wind speed	

Figure 3. MEDUSA sensors output and derived physical quantities.

the cumulative mass of smaller grains (see Figure 1).

Number density of particles vs. size. This measurement is related to the previous result through the sampling operations. Once particle counting and/or mass measurements have been performed, dust number density can be derived, since the volume sampled by the system is known. Due to the poor knowledge of the actual dust size distribution and number densities in Martian atmosphere, the instrument design considers sufficient margins to cope with a wide range of dust properties.

Water vapor abundance in the atmosphere. This measurement is basically independent from the previous ones. The cumulative mass measurement of the water vapor condensed on the sensing device in a defined interval and environment conditions (*p, T*) provides the water abundance monitoring.

Dust deposition, removal, suspension and electrification. The dust deposition rate on the sensor surface is measured by detecting scattered light. Similarly, dust removal can also be quantified, thus giving the opportunity to study granular entrainment mechanisms. By applying electric fields to the dust accumulation surface the electrification level of the suspended dust can be determined. Using patterned laser beams suspended dust velocities (speed and angle) can be determined, which quantifies the wind velocity (and the surface wind shear stress). From the measured wind speed and the suspended dust detection rate, the concentration of dust grains in the atmosphere can be obtained directly.

Long-term and short-term time evolution due to local events. This feature implies mainly operation requirements. The system shall repeat the sampling and analysis of variable amounts of atmosphere. Different environment conditions could result in different dust number densities by orders of magnitude.

Atmospheric dust sampling for other analytical measurements. Atmospheric dust could be sampled and delivered to other analytical experiments for characterization of chemical and physical dust properties, complementary to MEDUSA results.

Working principle

Optical detection. The Optical System is a single optical particle counter (OPC) that counts and measures size of grains passing through a small sensing zone illuminated by a laser. The system is dimensioned to minimize multiple detection (probability < 5%). The passing particle generates a pulse of scattered light, whose distribution vs. scattering angle q is function of particle physical properties, such as size, shape, orientation, size parameter a (for a sphere $a = 2pr_p / l$, where r_p is the particle radius and l is the wavelength of the incident light), complex refractive index ($m = n - ik$) of the particle material, l and polarization of the incident wave (Rader and O'Hern 2001). The scattered light is collected by 2 mirrors, in the forward (± 33°) and backward (± 47°) scattering directions, focusing it on two photodiodes. Particle counts and sizes are derived by means of calibration curves obtained for particles of known size. The choice of collecting scattering angles involves a trade-off of many factors. The forward direction has been chosen as, in this direction, the signal intensity mainly depends on scattering angle q and size parameter a and is less dependent on particle material (*i.e.*, *m*), so that particle size can be derived more easily. In turn, backward scattering intensity depends also on grain material. Therefore, an optimal scattering light detection system shall include simultaneous forward and backward detection to combine different information on the analyzed grain.

Cumulative mass detection. Cumulative dust mass detection is performed by a microbalance device (MBd). Microbalances are thermally stable piezoelectric transducers, whose frequency is proportional to the mass deposited on the sensor. The measured physical quantity is the shift of the resonant frequency *f* of a quartz oscillator (Stockbridge 1966). The use for dust collection requires a careful analysis of performances vs. dust physical and dynamical characteristics (Palomba et al. 2001; Palomba et al. 2002).

Water vapor measurement. Microbalances are also appropriate to measure quantitatively the mass of volatiles, *e.g.*, water vapor condensed onto the sensing crystal (Battaglia et al. 2004). The detection is achieved by cooling the crystal sensor under frost point by a Peltier device and by monitoring the deposition curve. Frosting signal associated to a certain crystal temperature allows obtaining the value of the atmospheric vapor partial pressure and the relative humidity at the time of measurement. The sensor temperature is measured with a platinum resistance element included in the MBwv at a frequency of about 20 Hz.

Dust accumulation and electrification measurements. By measuring the light scattered by the dust accumulated on a transparent surface, the dust deposition rate can be quantified. By applying an electric field to this surface the

4

enhancement/reduction of dust deposition allows studying the electrification of the suspended dust. By measuring light scattered by suspended grains velocity and, therefore, wind speed/direction can be quantified. Refer to Merrison et al. 2006 for a more detailed description.

Instrument architecture

MEDUSA is composed of the following subsystems (see Figure 4):

- The Main Body, including the dust sampling head (inlet), the optical detection system, the cumulative (dust) mass detection stage and the pump. The Optical System (OS) is placed below the inlet nozzle, followed by the cumulative (dust) mass detection stage (MBd). The pump is placed at the end of this chain to guarantee gas and dust flux through the system. This configuration allows the best sensitivity coverage, ranging over more than three orders of magnitude in grain size. The light source for the OS is a laser diode, located in a Laser Diode Assembly (LDA), to be accommodated outside the Main Body in a temperature benign environment. The light is transported to the OS via an optical fibre.

- The water vapor microbalance (MBwv), equipped with a Peltier device for cooling and thermal stabilization, is exposed to condense atmospheric water vapor, but protected in a case suitable to avoid dust deposition on the sensing crystal.

- The Dust Deposition and Electrification Stage (DDES) includes six lasers and deposition chargeable surfaces for dust deposition and electrification measurements.

- The instrument Main Electronics (ME).

Main Body. The Main Body is devoted to the sampling and measurements of dust in the atmosphere. The flux of gas and dust inside it is regulated by a pump. Gas and dust particles entering the sampling head (inlet) are conveyed to a cylindrical duct. An OS is located along the duct and allows the measurement of single dust grain size. The duct ends with a nozzle, in front of a cumulative dust mass detection stage (MBd), which measures the mass of accumulated dust. The sensing area of OS and MBd are similar so that the measurements performed with the two subsystems can be correlated.

The inlet is designed with cylindrical symmetry (Figure 4). It shall guarantee unbiased dust sampling from the atmosphere with the same efficiency on 360° horizontal angle, minimizing biases from wind direction. It shall minimize gas pressure variations on the path. The upper surface of MEDUSA inlet is a radiative sink to the sky temperature and a thermal flux interface. It acts also as a cap, avoiding the entrance of particles when the pump is off. The gas inlet is mechanically mounted on the upper part of the OS.

Optical System. A 3D model of the OS is shown in Figure 5. All components are accommodated inside a cylindrical envelope, with diameter of 130 mm, including also the
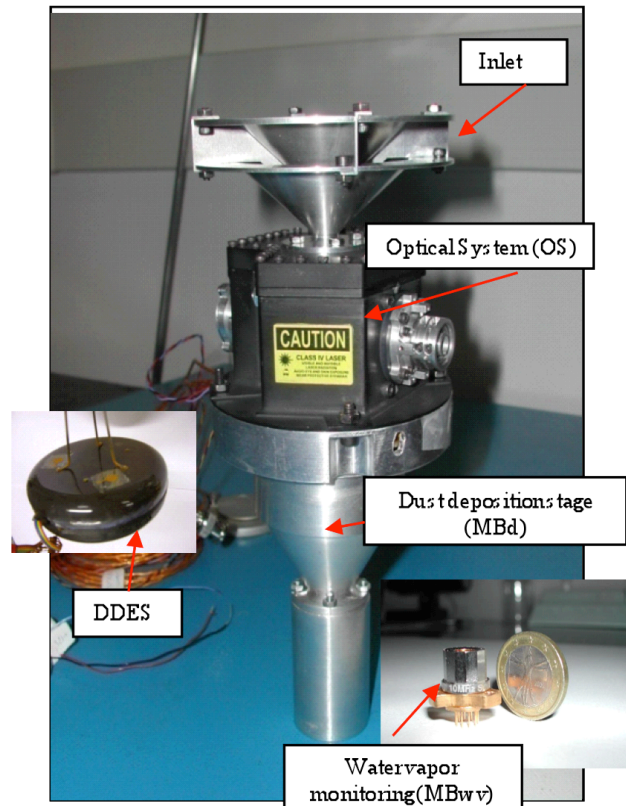

Figure 4. MEDUSA breadboard.

support and mechanical interfaces of the OS to the inlet (upper side) and to the proximity electronics (bottom side). The light source is a laser diode (l = 808 nm, optical power = 1 W). The anamorphic objective is constituted by a collimating lens and by cylindrical optics to provide the required beam shaping, in particular within the sampling volume. The sampling volume has been sized according to the expected particle density range (Metzger et al. 1999), to achieve meaningful sampling of Martian atmosphere. It is 8 ´ 3 ´ 0.2 mm^3 and has been designed according to the following requirements: a) a large enough number of particles ($\sim 10^4$) shall be detected in a short observation time (~ 100 s), *b*) to have a single particle counter the sampling volume shall be chosen in order to have small fraction F of coincidence events: $F \le 0.05$, *c*) to cope with a large range for the dust grain number density.

The OS optics collecting the scattered beams are reflective elements, allowing better performances with lower masses with respect to refractive optics. Two collecting mirrors are used, dedicated to collect the forward scattered and the backward scattered light, respectively. Both mirrors have a central hole to allow the accommodation of the anamorphic optics and the transit of the light beam, in the case of backward mirror, and the transit of the exiting "direct" light beam and the accommodation of a light trap, in the case of forward mirror. The trap collects the light power and dissipates it as heat, by conduction to the OS mechanical box. As an undesired phenomenon, a very small quantity of light power exits the light trap, and part of it reaches the detectors. This fractional power, referred to as stray-light, is
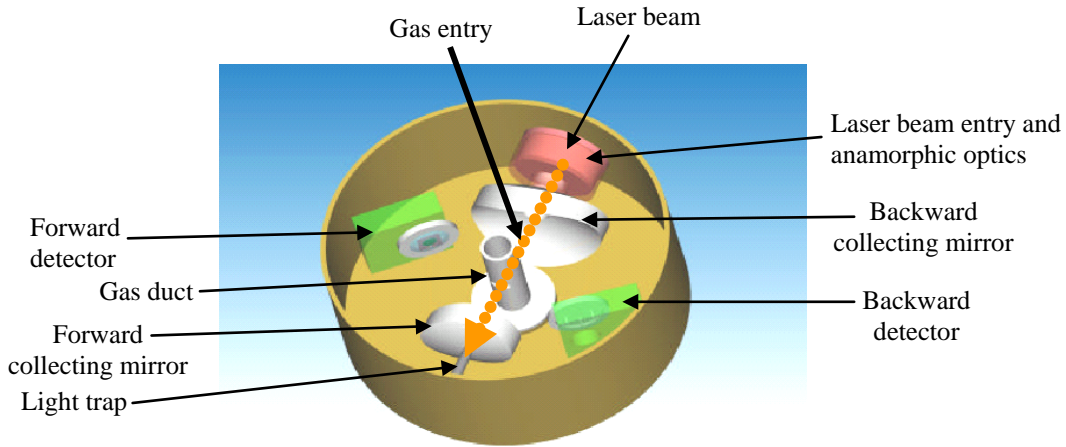
Figure 5. 3-D model of the optical sensor.

constant, being directly dependent on the laser diode emission, and generates a constant photocurrent in the detectors. For the detectors, silicon PIN photodiodes have been chosen. These devices exhibit low noise and good responsivity in the IR region selected for the MEDUSA source. Taking into account the expected dust grain size, the photodiodes of the two channels of the optical system provide output currents with a lower bound of few nA. Such low signals need to be amplified before being sent to the Main Electronics so to avoid that environmental noise added along the wires make them undistinguishable. As a consequence, the Proximity Electronics stage has been placed below the optical system, minimizing the length of the connections to the detectors.

Cumulative dust mass detection stage (MBd). The cumulative dust collection stage uses one microbalance device. MBd is located at the end of the gas duct. The baseline choice for the MBd is a 15 MHz MB (model MK21 by QCM Research) with 1.97×10^{-10} g/Hz sensitivity and 3×10^{-4} g dynamic range. This ensures more than 6000 runs (duration $\sim$ 100 s) in standard conditions (constant haze). During a dust storm, the duration of each run can be tuned in order to guarantee a large number of measurements before saturation.

QCM Research sensors are space qualified. The accommodation of the MBd inside the Main Body is shown in Figure 6. The device is composed of two quartz crystal oscillators. One of them is exposed to the dust environment.

Water vapor detection stage (MBwv). The MBwv is a separate microbalance, equipped with a Peltier device, for cooling and thermal stabilization. It is exposed to the Martian atmosphere to condense atmospheric water vapor. An external case (see Figure 7) is foreseen in order to protect the sensor from dust contamination and solar radiation. The configuration of the aperture is designed to prevent contamination by dust settling onto the sensor sensitive surface, while allowing free access to the environmental water vapor to be measured.

Recent measurements of water vapor abundance (Smith et al. 2009) show an annual variability of water vapor abundance ranging around 5×10^{-4} - 5×10^{-3} mbar. This corresponds to a frost temperature in the range from about -65 to -80 °C. So, a temperature controlled microbalance, operating with $\Delta T = -90$ °C, allows the detection of water vapor in each condition (if the MBwv crystal temperature is equal to the atmospheric one). In fact, with such ΔT, the frost temperature is reached under almost all temperature and abundance conditions starting from the maximum expected atmospheric temperature $T = 0$ °C. The baseline choice for the MBwv is the MK20-4 model by QCM Research, including 3 Peltier
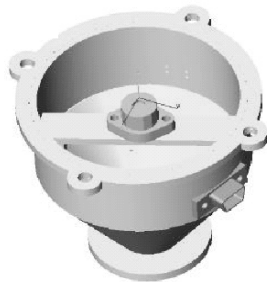

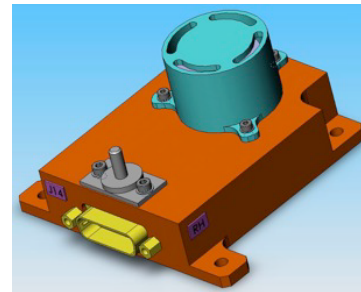**Figure 6**: MBd inside the Dust Collector stage in the Main Body.

Figure 7. 3D model of the MBwv unit.

6

stages, matching the required D*T* requirement. This sensor is space qualified.

Dust Deposition and Electrification stage (DDES). The DDES (Dust Deposition and Electrification Stage) is another separate stage and includes 6 lasers and transparent electrodes for dust deposition/removal and dust electrification measurements. In addition, this sensor can detect individual suspended dust grains and quantify the wind speed and dust concentration. A full description of DDES is reported in Merrison et al. (2006).
The present mass of the instrument is about 1990 g, with a maximum power consumption of 19.6 W and a total energy consumption per sol of 18.7 Wh.

All the sensing subsystems forming MEDUSA have been or are being tested at MEDUSA team's laboratories; some of them (OS, MBd) are identical to or directly derived from sensor already in use for space missions (Colangeli et al. 2007).

Performance and status

A breadboard of the MEDUSA instrument was built and tested under ESA and Italian Space Agency (ASI) contracts. Here we report some of the most interesting results.

Tests on the microbalance for dust (MBd) detection. Tests have been performed on a custom microbalance. Technical characteristics are reported in Table 1.

Table 1. Datasheet of the MB for dust measurements.

Storage Temperature	-65 to 100 °C
Operating Temperature Range	-40 to 100°C
Temperature Sensor	NTC Thermistor 10KW @ 25 °C
Crystal Resonance Frequency	15 MHz
Nominal Mass Sensitivity	1.96×10^{-9} g Hz^{-1} cm^{-2}
Nominal Frequency Saturation Limit	150 KHz
Weight	7.5 g
Power Supply	5 V to 18 V

The sensor dependence on the temperature has been evaluated. By varying the temperature, it has been observed a variation in the resonance frequency. The MB has been placed in a clean chamber, in which a high vacuum, down to 10^{-5} mbar, has been produced. MB has been passively cooled and heated through its heat sink in a temperature range from -85 to +58 °C. Hence, the test has been performed in order to obtain a close thermal cycle. In this way it has been possible to evaluate the "hysteresis" effect in the calibration curve. Different close thermal cycles have been applied, to check for repeatability. The calibration curve presents some reproducible hysteresis values (Figure 8).

Moreover, the MBd has been calibrated versus the mass of deposited particles. This performance test is based on the measurement of the output frequency of MBd for known concentrations of deposited dust. Sample used is the JSC-
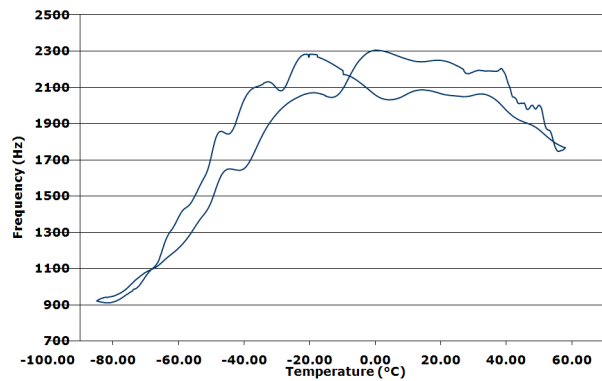

Figure 8. Frequency vs. temperature of the MB for dust measuremements. Example of applied thermal cycles.

Mars-1, as a good analogue of the dust expected in the Martian environment. Sensitivity, linearity response and saturation point have been evaluated. The sample material has been ground and sieved in order to obtain grain sizes similar to those expected in the Martian lower atmosphere (< 20 μm). Then, grains have been suspended in pure water in known concentration. Calibrated volumes of suspension have been deposited on the active area of the MBd crystal sensor. Suspension concentration has been set in order to obtain a shift in MB resonant frequency of 1 kHz per μl of deposited suspension. Measurements have been performed after water complete evaporation. Deposition of suspension has been repeated up to the saturation of the MBd sensor.

The measured sensitivity is $(1.29 \pm 0.39) \times 10^{9}$ Hz g^{-1}, that is about 25% of the nominal value. This is due to the presence of dust grains with diameter larger than 10 μm. Particles with dimensions larger than a few μm are generally badly coupled with the surface of the sensor (Daley and Lundgren 1975; Palomba et al. 2002). MBd response results are linear with $R^2 = 0.9952$ (Figure 9).

Tests on the microbalance for water vapor (MBwv) detection. Tests on MBwv are based on the measurement of the vibration frequency of the MBwv for known concentrations of water vapor, by fixing the water vapor partial pressure at know values and by varying the sensor temperature. These tests have been performed under Martian
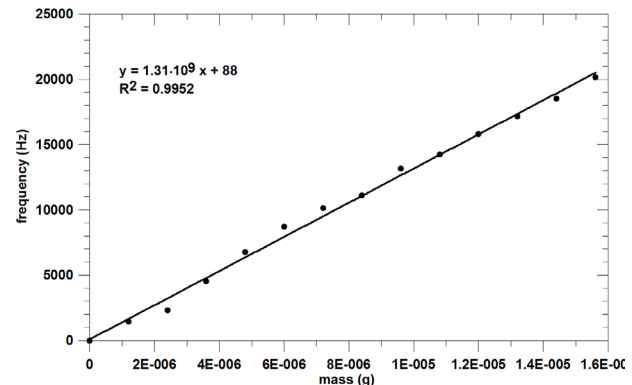

Figure 9. Mass vs. frequency plot. The values have been scaled to zero-frequency in clean electrode conditions. The sensitivity behavior, until saturation, is well fitted by a straight line.

7

water vapor partial pressure simulated conditions. The results are shown in Table 2 and show a good agreement between the measured and the expected frost temperature.

Table 2. Results of the water vapor condensation test for the MK20-2 QCM at three different vapor pressures and for different temperature rates.

Water vapour pressure (mbar)	Temperature rate (K/min)	Measured temperature (K)	Nominal frost point (K)
2.6×10^{-3}	10	203.06	203.15
	5	202.02	
5.5×10^{-4}	10	192.18	193.15
	5	192.47	
1.4×10^{-4}	10	184.61	185.15
	5	184.14	

Tests on the Optical System (OS). OS performances were evaluated by measuring the output voltage generated by spherical mono-dispersed particles injected in the system. Measurements have been repeated for four different sets of grains with radii: 0.5 μm, 2.5 μm, 5 μm and 20 μm, respectively. The former two sets are melamine resin particles (MF-R-1450 and MF-R-2750, respectively) from Micro particles GmbH. The 20 μm (radius) set contains glass microspheres (Soda Lime) by Duke Scientific Corporation.

Particles were injected into the instrument by using a custom device with compressed gas to disperse small amount of particles with a proper dilution.

The light source used during the test campaign is a laser diode series 2350 by JDSU. It works at a wavelength of 800-812 nm with an optical power of 0.5 W (against the nominal power of 1 W). Its far field energy distribution has a FWHM of 32° in the perpendicular plane and 12° in the parallel plane, respectively. A stray light optimization was achieved by using diaphragms and by implementing a stray light compensation mode on the OS proximity electronics (Molfese et al. 2010).

The optical power acquired by the two photodiodes were obtained from the measured voltage signals, through the photodiode conversion factor and then compared to theoretical values, predicted by Mie's theory. Results are plotted in Figure 10. Data fit with the Mie prediction considering a power density $D = 0.2$ W/mm^2 in the sampling volume.

Test campaign showed how critical is the coupling of the laser source and optics with respect to both stray light generation and reduction of laser source power density; nevertheless the performance tests demonstrated that this sub-system was able to detect single particles with radii < 0.5 μm. This is very close to the OS nominal performance (detection limit: 0.2 μm). In the case the nominal power density is reached, this limit corresponds to the detection of 0.2 μm particles.

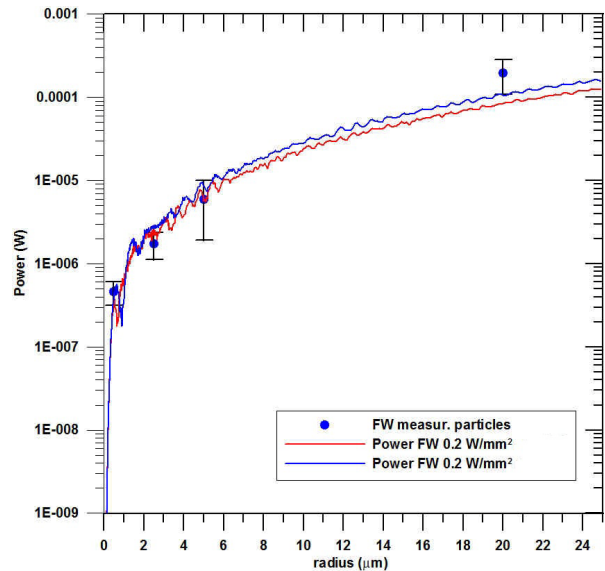The design of OS has been further improved by using a laser

Figure 10. Power predicted by the Mie's theory. Red and blue curves are Mie theoretical curves for melamine and Soda Lime particles, respectively. The behavior is compatible with a power density of 0.2 W/mm².
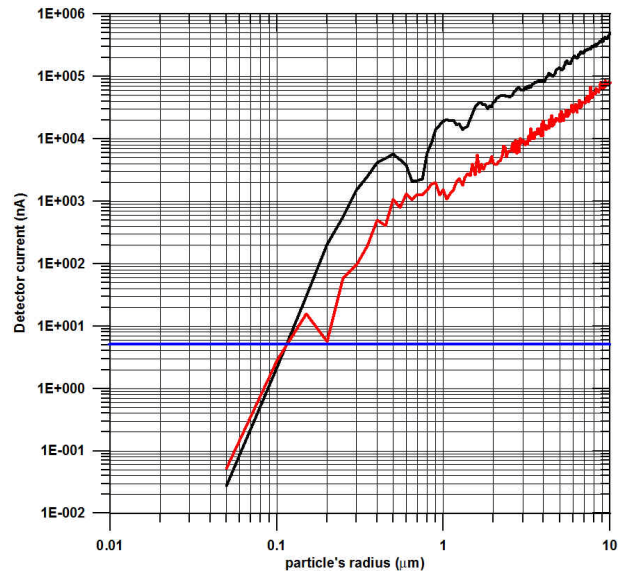

Figure 11. OS detector current intensity for forward and backward scattering. Detector dark current limit (5 nA) is shown for reference.

diode equipped with optic fiber; this approach allowed us to minimize stray light and maximize the optical power density. Moreover this new configuration offers the flexibility to place the laser source far from the instrument body, in an environment warmer than the Martian open atmosphere. With this new design the stray light was highly reduced (the measured voltage at the PE low gain output due to stray light is ~250 mV for FW channel and ~520 mV for BW channel) and the power density in the sampling volume maximized (~7500 mW/mm^2).

Starting from the measured optical power in the sampling

volume and the Mie's theory it can be shown that the minimum detectable particle radius is below 0.1 μm both in forward (FW) and in backward (BW) scattering (Figure 11).

Test campaign has been conducted by injecting spherical particles with different sizes into the MEDUSA OS to verify the performances. Measurements will be repeated using also non-spherical particles. We expect a deviation with respect to the Mie predictions mostly for particles with radii *r* in the range 0.1 – 1 mm. For *r* > 1 mm the scattered intensity is proportional to the particle cross-sectional area ($I \mu d^2$) and not strongly dependent on shape or composition for aspect ratios close to one (in particular for the FW scattering) (Rader and O'Hern 2001). A calibration curve will be derived starting from these results.

Tests on the Dust Deposition, Suspension and Electrification Sensor (DDES). This laser based opto-electronic device has been developed at the University of Aarhus. It constitutes an integration of three prototype sensors: a dust deposition/removal sensor, a dust electrification sensor and a laser anemometer. The DDES has been tested extensively under Mars Simulation conditions using Mars analogue dust (grain diameter around 2 mm) in the Aarhus Mars simulation wind tunnel, specifically low pressures (around 10 mbar) and varying wind speeds (0.2 - 15 m/s), dust concentrations (1 to 1000 particulates/cm^3) and instrument orientation (relative wind angle). During the test campaign the following parameters have been measured:

• Dust deposition rate (depending on the dust suspension conditions)

• Dust grain electrification (positive and negative)

• Suspended dust concentration

• Wind flow (speed and wind angle)

The measured values agree with previous determination made under the same simulation conditions and using direct optical analysis and/or Laser Doppler Anemometer (LDA) techniques.

Dust deposition is accurately quantified at six places on the instrument by detecting laser light scattered into photo-detectors. Some results are reported in Figure 12.

Electric fields are applied to the dust accumulator surface using a variable high voltage source and transparent electrodes made by vapor deposition of indium oxide. Both positive and negative electrodes are used in order to determine the fraction and degree of electrification of the
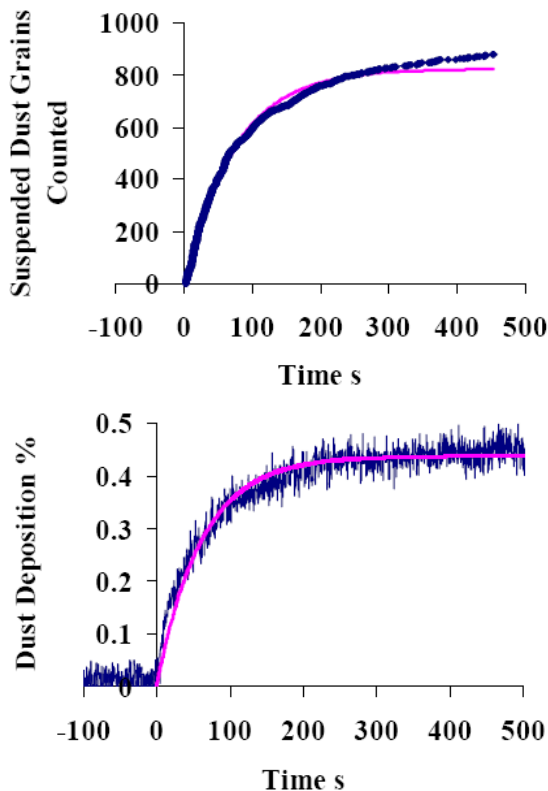

Figure 12. (Top) The integrated number of suspended dust grains counted by the LDA. (Bottom) The accumulated dust deposition, in fractional area coverage, measured by the DDES prototype instrument following Mars analogue dust injection into the Aarhus Wind Tunnel Simulator (AWTS).
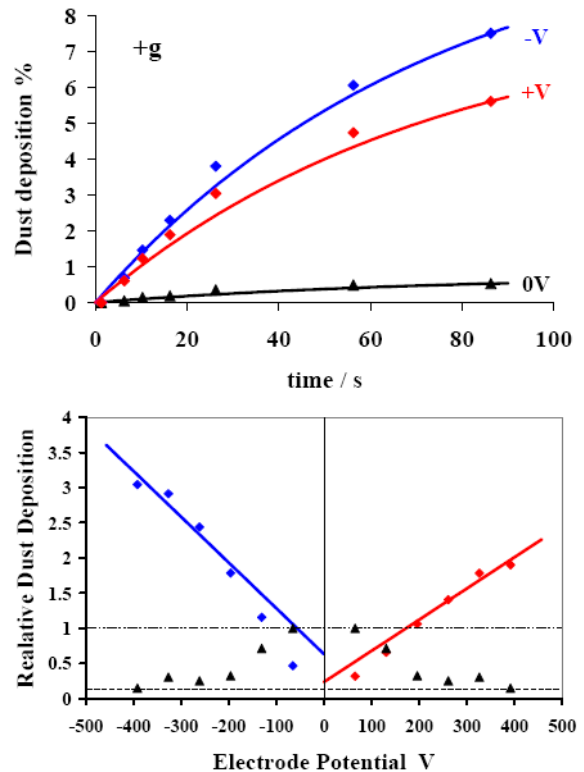

Figure 13. The upper plot shows the dust deposition measured by DDES and converted into percentage coverage for positive, negative (300 V) and an unbiased electrode again showing the large difference in dust accumulation rate. The lower plot shows a normalized set of deposition rates measured by DDES at different electrode voltages. Measurement of the gradient of these curves is the quantity used to determine the grain charge.
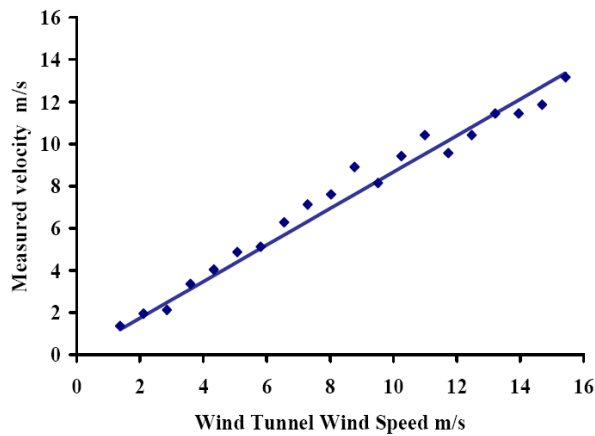
9

Figure 14. Wind velocity as measured by the DDES operated in the Mars simulation chamber vs. wind tunnel wind speed.
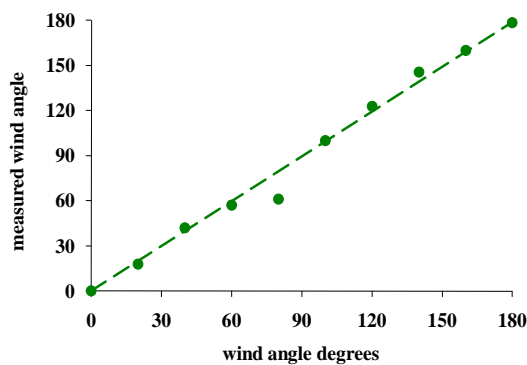

Figure 15. Wind angle measured by the DDES at different instrument orientations with respect to the wind.

Table 2. Performances of MEDUSA subsystems.

Subsystem	Measured quantity	Sensitivity	Saturation
OS	Single particle size (nm)	0.2	~ 100
OS	Particle number density (cm^{-3})	<< 1	~ 500
MBd	Cumulative mass of dust (kg)	2×10^{-13}	2×10^{-9}
MBwv	Water vapor abundance (ppb)	1	Saturation in atmosphere
DDES*	Dust deposition (%)	1	100
DDES	Dust electrification (e$^-$)	10^3	10^6
DDES	Wind speed (ms^{-1})	2	20

*100% dust deposition corresponds to the signal obtained after the deposition of an optically opaque (several mm thick) layer of dust.

dust (Figure 13).

Patterned laser beams are created using holographically generated interference gratings. Dust grains crossing the pattern (three lines in this case) generate a time varying light scattered signal which is collected using a Fresnel lens and detected using a photodiode. This time of flight system quantifies the wind velocity and the detection rate measures the suspended dust concentration (Figure 14). The wind angle (0 - 180º) can be determined from three of the velocity sensor measurements (*U*1, *U*2 and *U*3) oriented at 60º to each other, *i.e., $Angle = \arctan\left(\left(U3^2 - U2^2\right)/\left(1732 \times U1^2\right)\right)$* (see Figure 15). The wind speed can now be determined by $U = U1/\cos(Angle)$.

Performances of MEDUSA subsystems are summarized in Table 2.

Conclusions

Airborne dust and water vapor monitoring at the surface of Mars has a key role in the study of the climate and the physics of the atmospheric boundary layer of Mars, in searching for water surface reservoirs and in the hazard evaluation related to future robotic and/or manned space missions. The MEDUSA instrument is a suite of sensors for the direct and in situ measurements of dust size distribution, number density, deposition rate and electrification, and water vapor abundance at the surface level. It has actually reached a Technical Readiness Level > 5 within the European ExoMars mission development and is well suited to be accommodated on Martian landers and/or rovers.

Acknowledgements

References

Battaglia, R. et al. (2004) "Development of a micro-balance system for dust and water vapour detection in the Mars atmosphere" Advances in Space Research 33, 12, 2258-2262. doi:10.1016/S0273-1177(03)00520-9

Bourke, M. C. et al. (2008) "Recent aeolian dune change on Mars" Geomorphology 94, 1-2, 247-255. doi:10.1016/j.geomorph.2007.05.012

Cantor, B. et al. (2002) "Multiyear Mars Orbiter Camera (MOC) observations of repeated Martian weather phenomena during the northern summer season" Journal of Geophysical Research 107, 5014. doi:10.1029/2001JE001588

Chojnacki, M. et al. (2010) "Recent dune changes at Endeavour Crater, Meridiani Planum, Mars, from orbital observations" Lunar and Planetary Science XLI, 2326.

Colangeli, L. et al. (2007) "The Grain Impact Analyser and Dust Accumulator (GIADA) experiment for the Rosetta mission: Design, performances and first

results" Space Science Reviews 128, 1-4, 803-821. doi:10.1007/s11214-006-9038-5

Daley, P. S. and D. A. Lundgren (1975) "The performance of piezoelectric crystal sensors used to determine aerosol mass concentrations" American Industrial Hygiene Association Journal 36, 518. doi:10.1080/0002889758507285

Drossart, P. et al. (1991) "Martian aerosol properties from the Phobos/ISM experiment" Annales Geophysicae 9, 754-760.

Fedorova, A. et al. (2006) "Mars water vapor abundance from SPICAM IR spectrometer: Seasonal and geographic distributions" Journal of Geophysical Research 111, E09S08. doi:10.1029/2006JE002695

Fedorova, A. A. et al. (2009) "Solar infrared occultation observations by SPICAM experiment on Mars-Express: Simultaneous measurements of the vertical distributions of H_2O, CO_2 and aerosol" Icarus 200, 96-117. doi:10.1016/j.icarus.2008.11.006

Fenton, L. K. (2006) "Dune migration and slip face advancement in the Rabe Crater dune field, Mars" Geophysical Research Letters 33, L20201. doi:10.1029/2006GL027133

Forget, F. et al. (2006) "Climates and storms" in Planet Mars – Story of another world. Springer 137-139.

Fouchet, T. et al. (2007) "Martian water vapor: Mars Express PFS/LW observations" Icarus 190, 32-49. doi:10.1016/j.icarus.2007.03.003

Greeley, R. and J. D. Iversen (1985) "Wind as a geological process on Earth, Mars, Venus and Titan" Cambridge Planetary Science Series 4. Cambridge University Press, Cambridge.

Greeley, R. et al. (1992) "Martian aeolian processes, sediments, and features" in Mars (H. H. Kieffer, B. M. Jakosky, C. W. Snyder and M. S. Mathews editors) 730-766, University of Arizona Press, Tucson.

Iversen, J. D. (1982) "Saltation threshold on Earth, Mars and Venus" Sedimentology, 29, 1, 111-119. doi:10.1111/j.1365-3091.1982.tb01713.x

Jakosky, B. M. and C. B. Farmer (1982) "The seasonal and global behavior of water vapor in the Mars atmosphere - Complete global results of the Viking atmospheric water detector experiment" Journal of Geophysical Research 87, 2999-3019. doi:10.1029/JB087iB04p02999

Jakosky, B. M. and R. M. Haberle (1992) "The seasonal behavior of water on Mars" in Mars (H. H. Kieffer, B. M. Jakosky, C. W. Snyder and M. S. Mathews editors) 969-1016, University of Arizona Press, Tucson.

Jakosky, B. M. and T. Z. Martin (1987) "Mars - North-Polar atmospheric warming during dust storms" Icarus 72, 528-534. doi:10.1016/0019-1035(87)90050-9

James, P. B. et al. (1992) "The seasonal cycle of carbon dioxide on Mars" in Mars (H. H. Kieffer, B. M. Jakosky, C. W. Snyder and M. S. Mathews editors) 934-968, University of Arizona Press, Tucson.

Kahn, R. A. et al. (1992) "The Martian dust cycle" in Mars (H. H. Kieffer, B. M. Jakosky, C. W. Snyder and M. S. Mathews editors) 1017-1053, University of Arizona Press, Tucson.

Malin, M. C. and K. S.Edgett (2001) "Mars Global Surveyor Mars Orbiter Camera: Interplanetary cruise through primary mission" Journal of Geophysical Research 106, 23429-23570. doi:10.1029/2000JE001455

Martin, T. Z. and H. H. Kieffer (1979) "Thermal infrared properties of the Martian atmosphere. II - The 15-micron band measurements" Journal of Geophysical Research 84, 2843-2852. doi:10.1029/JB084iB06p02843

Martin, T. Z. (1981) "Mean thermal and albedo behavior of the Mars surface and atmosphere over a Martian year" Icarus 45, 427-446. doi:10.1016/0019-1035(81)90045-2

Melchiorri, R. et al. (2007) "Water vapor mapping on Mars using OMEGA/Mars Express" Planetary and Space Science 55, 3, 33-342. doi:10.1016/j.pss.2006.05.040

Merrison, J. et al. (2004) "The electrical properties of Mars analogue dust" Planetary and Space Science 52, 4, 279-290. doi:10.1016/j.pss.2003.11.003

Merrison, J. P. et al. (2006) "An integrated laser anemometer and dust accumulator for studying wind-induced dust transport on Mars" Planetary and Space Science 54, 11, 1065-1072. doi:10.1016/j.pss.2006.05.026

Merrison, J. P. et al. (2007) "Determination of the wind induced detachment threshold for granular material on Mars using wind tunnel simulations" Icarus 191, 568-580. doi:10.1016/j.icarus.2007.04.035

Metzger, S. M. et al. (1999) "Dust devil vortices seen by the Mars Pathfinder camera" Geophysical Research Letters 26, 2781-2784. doi:10.1029/1999GL008341

Molfese, C. et al. (2010) "Stray light compensation for dust analysers based on light scattering" Proceedings SPIE, 7726, 77261A. doi:10.1117/12.853438

Moroz, V. I. et al. (1993) "Spectrophotometry of Mars in the KRFM experiment of the PHOBOS mission: Some properties of the particles of atmospheric aerosols and the surface" Planetary and Space Science 41, 569-585. doi:10.1016/0032-0633(93)90077-F

Palomba, E. et al. (2001) "The sticking efficiency of quartz crystals for cosmic sub-micron grain collection" Planetary and Space Science 49, 919-926. doi:10.1016/S0032-0633(01)00015-0

Palomba, E. et al. (2002) "Performance of micro-balances for dust flux measurement" Advances in Space Research 29, 8, 1155-1158. doi:10.1016/S0273-1177(02)00131-X

Pollack, J. B. et al. (1995) "Viking Lander image analysis of Martian atmospheric dust" Journal of Geophysical Research 100, 5235-5250. doi:10.1029/94JE02640

Rader, D. J. and T. J. O'Hern (2001) "Optical direct-reading techniques: in situ sensing" in Aerosol measurement: principles, techniques, and applications (P. A. Baron and K. Willeke editors) 455–494, John Wiley and Sons, New York.

Rosenqvist, J. et al. (1992) "Minor constituents in the Martian atmosphere from the ISM/Phobos experiment" Icarus 98, 254-270. doi:10.1016/0019-1035(92)90094-N

Ryan, J. A. and R. M. Henry (1979) "Mars atmospheric phenomena during major dust storms, as measured at surface" Journal of Geophysical Research 84, 2821-2829. doi:10.1029/JB084iB06p02821

Saruya, T. et al. (2010) "The exchanges of water vapor between the atmosphere and the surface of Mars" Lunar and Planetary Science XLI, 1306.

Silvestro, S. et al. (2010) "Ripple migration and small ,odifications of active dark dunes in Nili Patera (Mars)" Lunar and Planetary Science XLI, 1820.

Smith, M. D. (2002) "The annual cycle of water vapor on Mars as observed by the Thermal Emission Spectrometer" Journal of Geophysical Research 107, 5115. doi:10.1029/2001JE001522

Smith, M. D. et al. (2004) "First atmospheric science results from the Mars Exploration Rovers Mini-TES" Science 306, 1750-1753. doi:10.1126/science.1104257

Smith, M. D. (2008) "Spacecraft observations of the Martian atmosphere" Annual Review of Earth and Planetary Sciences 36, 191-219. doi:10.1146/annurev.earth.36.031207.124334

Smith, M. D. et al. (2009) "Compact Reconnaissance Imaging Spectrometer observations of water vapor and carbon monoxide" Journal of Geophysical Research 114, E00D03. doi:10.1029/2008JE003288

Smith, P. H. et al. (2009) "H_2O at the Phoenix landing site" Science 325, 58. doi:10.1126/science.1172339

Stockbridge, C. D. (1966) "Effects of gas pressure on quartz crystal microbalances" in Vacuum Microbalance Techniques (K. Behrndt editor) 147, Plenum, New York.

Titov, D. V. et al. (1999) "Measurements of the atmospheric water vapor on Mars by the Imager for Mars Pathfinder" Journal of Geophysical Research 104, 9019-9026. doi:10.1029/1998JE900046

Tomasko, M. G. et al. (1999) "Properties of dust in the Martian atmosphere from the Imager on Mars Pathfinder" Journal of Geophysical Research 104, 8987-9008. doi:10.1029/1998JE900016

Toon, O. B. et al. (1977) "Physical properties of the particles composing the Martian dust storm of 1971-1972" Icarus 30, 663-696. doi:10.1016/0019-1035(77)90088-4

Tschimmel, M. et al. (2008) "Investigation of water vapor on Mars with PFS/SW of Mars Express" Icarus 195, 557-575. doi:10.1016/j.icarus.2008.01.018

Whiteway, J. A. et al. (2009) "Mars water-ice clouds and precipitation" Science 325, 68. doi:10.1126/science.1172344

Zimbelman, J. R. (2000) "Non-active dunes in the Acheron Fossae region of Mars between the Viking and Mars Global Surveyor eras" Geophysical Research Letters 27, 1069-1072. doi:10.1029/1999GL008399

Zurek, R. W. et al. (1992) "Dynamics of the atmosphere of Mars" in Mars (H. H. Kieffer, B. M. Jakosky, C. W. Snyder and M. S. Mathews editors) 835-933, University of Arizona Press, Tucson.

Zurek, R. W. and L. J. Martin (1993) "Interannual variability of planet-encircling dust storms on Mars" Journal of Geophysical Research 98, 3247-3259. doi:10.1029/92JE02936